Vol. 2 No. 4 (2025)
ONLINE ISSN :3007-309X
PRINT ISSN :3007-3081
Journal of Medical & Health Sciences Review

OPTIMIZING ROTATIONAL ANGLE ASSESSMENT IN ACETABULAR FRACTURE THROUGH JUDET VIEW IN X-RAY IMAGING

Ali Raza[1], Kiran Aslam[2], Safura[3], Deedar Ali Jamro[4], Zubeda Nangrejo[5], Faiza Ali[6], Ghulam Ali jamro[7]

[1]Institute of Physics, The Islamia University of Bahawalpur, Pakistan
Email: alirazauos.edu.pk@gmail.com
[2]Institute of Physics (IOP), The Islamia University of Bahawalpur (IUB), Pakistan,
Email: kiranaslam0091@gmail.com
[3]Senior Lecturer, Department of Radiology, Kalam Bibi International Women Institute, Bannu, Pakistan, Email: safurasultan96@gmail.com
[4]Department of Physics and Electronics,Shah Abdul Latif University Khairpur, Pakistan
Email: deedar.jamro@salu.edu.pk
[5]Department of Physics and Electronics, Shah Abdul Latif University, khairpur, Pakistan,
Email: zubeda.nangrejo@salu.edu.pk
[6]Department of Operation Theatre Technology, Riphah International University, Lahore, Pakistan, Email: faiza.ali@riphah.edu.pk
[7]Department Physics and Electronics, Shah Abdul Latif University, Khairpur, Pakistan
Email: galijamro@gmail.com

ARTICLE INFO:

Keywords:
Acetabular Fractures, Judet View, X-Ray Imaging, Rotational Angle, Imaging Protocolsinter- Observer Agreement, Measurement Errors.

Corresponding Author:
Ali Raza, Institute of Physics, The Islamia University of Bahawalpur, Pakistan
Email: alirazauos.edu.pk@gmail.com

Article History:
Published on 15 December, 2025

ABSTRACT

Accurate assessment of acetabular fractures is crucial for effective treatment. The Judet view, a specialized X-ray projection, is essential for evaluating fracture morphology. However, inconsistent rotational angles during imaging can lead to inaccurate assessments. This study investigates the optimal rotational angle for Judet view X-ray imaging in acetabular fracture assessment. We analyzed 25 cases, comparing rotational angles of 10°, 20°, 30° and 45° to determine the most accurate angle for fracture visualization. Our results indicate that a 45° rotational angle provides the most reliable assessment of fracture morphology, improving inter-observer agreement and reducing measurement errors. Standardizing the Judet view X-ray protocol with this optimal angle can enhance diagnostic accuracy and inform treatment decisions for acetabular fractures. Our study analyzed 25 acetabular fracture cases, comparing Judet view X-ray images taken at rotational angles of 10°, 20°, 30° and 45o. We evaluated fracture visualization, inter-observer agreement, and measurement errors. This study demonstrates that optimizing the rotational angle in Judet view X-ray imaging significantly enhances the assessment of acetabular fractures. Our findings suggest that a 45° rotational angle provides the most accurate

visualization of fracture morphology, improves inter-observer agreement, and reduces measurement errors.

1. Introduction

Acetabular fractures are among the most complex orthopedic injuries to diagnose and manage due to the intricate anatomy of the pelvis and its critical role in supporting hip stability and mobility(Kelly, Ladurner, & Rickman, 2020). These fractures typically result from high-energy trauma, such as road traffic accidents or falls from significant heights. Because the acetabulum forms the socket of the hip joint and bears substantial load, an accurate diagnosis is essential to prevent long-term complications including avascular necrosis, post-traumatic arthritis, and chronic hip instability(Tigani et al., 2025). Precise evaluation is also vital for surgical planning, as many fracture patterns involve the weight-bearing surface of the joint, where even minor misinterpretations can compromise patient outcomes(Popa et al., 2024).

Radiographic imaging plays a central role in the assessment of acetabular fractures, and among the available modalities, the Judet view X-ray remains a key diagnostic tool(Tazeabadi et al., 2020). Named after Robert and Jean Judet, this technique uses two specific oblique projections of the pelvis—the iliac oblique and the obturator oblique views. Together, these projections allow clearer visualization of the anterior and posterior walls of the acetabulum, the location and displacement of fracture fragments, and critical structures such as the quadrilateral plate(Dreizin, LeBedis, & Nascone, 2019). Despite its clinical importance, the effectiveness of the Judet view relies heavily on proper pelvic rotation during image acquisition. Any deviation due to patient discomfort, operator error, or equipment variability can distort key structures, making fracture lines difficult to interpret(Mercer & Stewart, 2019).

Currently, there is no universally accepted standard for the rotational angle required to consistently produce optimal Judet view images(Martinec & Pajdla, 2007). This lack of standardization results in inconsistencies across clinical settings, potentially affecting diagnostic accuracy and surgical planning. Variations in rotational angles may obscure important anatomical details, increasing the chance of misinterpretation and leading to errors in treatment decisions. Consequently, clinicians often face challenges when evaluating images that do not adequately reveal the full extent of the fracture(Morgenstern et al., 2018).

In response to these challenges, the present study aims to systematically investigate the influence of different rotational angles on the quality of Judet view X-ray images. By identifying the angle that provides the clearest visualization of acetabular fracture patterns, the study seeks to enhance diagnostic precision and reduce the variability commonly observed in clinical practice(Castaneda et al., 2015). Standardizing this aspect of the imaging technique may contribute to more reliable assessments, improved inter-observer agreement, and better alignment of treatment decisions with fracture morphology. Ultimately, optimizing Judet view imaging has the potential to improve diagnostic efficiency, strengthen clinical decision-making, and enhance patient outcomes in the management of acetabular fractures(Teja, Shrivastava, Choudhary, Rathod, & Balusani, 2024).

2. Methodology

2.1 X-Rays

X-rays are a form of electromagnetic radiation widely used in medical imaging to visualize internal tissues. When an X-ray beam passes through the body, dense structures such as bone

absorb more radiation than soft tissues, creating contrast on the image receptor. This contrast produces a clear two-dimensional view of skeletal structures(Glaser et al., 2015).

In the assessment of acetabular fractures, X-rays provide essential information on fracture patterns, fragment displacement, joint involvement, and alignment. The Judet view, in particular, offers an oblique perspective of the acetabulum, enabling improved visualization of fracture lines and guiding treatment planning.

2.2 Applications of X-Rays

X-rays play a central role in clinical radiology due to their ability to non-invasively assess internal structures. In diagnostics, they help detect bone fractures, chest infections, and abdominal abnormalities such as renal stones or intestinal obstruction. In therapeutic settings, X-rays assist in radiation therapy to target tumors.

Orthopedic surgeons rely on X-rays to confirm fracture alignment, guide treatment decisions, and evaluate healing. X-ray guidance is also used in minimally invasive procedures such as biopsies and angioplasties. Their wide utility, rapid acquisition, and affordability make them indispensable in modern medicine(Garbe & Sharma, 2024).

2.3 Image Acquisition

X-ray images will be captured using a **digital radiography system (Discovery XR656, GE Healthcare)** under standardized parameters to ensure consistency:

- Beam energy: **60–120 kVp**
- Matrix size: **2048 × 2048 pixels**
- Exposure time: **10–20 ms**
- Pixel size: **0.15 × 0.15 mm**

Patients will be positioned supine, with the affected hip centered on the receptor. The X-ray beam will be aligned to the acetabulum, and the **Judet view (45° oblique)** will be obtained.

All images will be saved in **DICOM format** and transferred to a dedicated workstation for analysis. Standardized acquisition minimizes variability and ensures accurate angle measurements.

2.4 Image Processing and Analysis

DICOM images will be analyzed using **ImageJ (NIH)**. Image quality will be enhanced using a **3×3 Gaussian filter**, while the **Sobel operator** will assist in edge detection. Manual segmentation of the acetabulum and fracture fragments will be performed using a pointer tool.

A custom script will calculate the rotational angle (α) between the acetabular axis and displaced fragment. The acetabular axis will be defined by connecting the centers of the acetabular circles. The angle will be measured by comparing **Line A (acetabular axis)** and **Line B (fragment line)**. Measurements will be exported to Excel for statistical analysis. Two independent observers will assess images to ensure reliability, and phantom models will be used to validate measurement accuracy.

2.5 Error Reduction and Optimization

Multiple techniques will be applied to enhance accuracy:

- **Image enhancement:** Filters reduce noise and improve clarity.
- **Automated landmark detection:** Minimizes human error using algorithms.
- **Multi-view analysis:** Combining AP and Judet views improves precision.
- **Iterative measurements:** Repeated measurements reduce random error.

- **Machine learning:** Models may be trained for angle prediction.
- **Observer training:** Improves inter-observer consistency.
- **Phantom studies:** Validate accuracy using known rotational angles.
- **Quality control:** Ensures standardized and reliable imaging output.

These steps collectively improve precision in rotational angle measurement.

2.6 Statistical Analysis

Statistical tools will be used to evaluate measurement accuracy and reliability:

- **Descriptive statistics:** Mean, median, SD of angle measurements.
- **Intraclass Correlation Coefficient (ICC):** Measures observer agreement.
- **Bland–Altman plots:** Assess agreement between methods.
- **Regression analysis:** Determines correlations with fracture characteristics.
- **ANOVA/t-tests:** Compare means among fracture groups.
- **ROC analysis:** Evaluates diagnostic accuracy and cut-off points.
- **Kappa statistics:** Measures agreement in angle categories.
- **Bootstrap resampling:** Estimates confidence intervals.

These techniques validate the robustness of the measurement method.

2.7 Validation and Reliability Testing

To ensure accuracy, several validation strategies will be used:

- **Ground truth comparison:** Using CT scans or intraoperative findings.
- **Intra- and inter-observer testing:** Assesses measurement repeatability.
- **Test-retest reliability:** Repeated imaging evaluates consistency.
- **Phantom studies:** Provide controlled validation using pre-set angles.
- **Clinical validation:** Compares measurements with surgical outcomes.
- **Comparison with existing methods:** Benchmarks performance.
- **Sensitivity and specificity:** Determine diagnostic accuracy.
- **Reliability coefficients:** ICC and kappa values will be calculated.

These evaluations ensure the method is precise, accurate, and reproducible.

2.8 Cassette

An X-ray cassette securely houses the film or digital detector. It includes a **light-tight enclosure** to prevent exposure, **intensifying screens** to boost image brightness, and a **firm holder** that keeps the film or sensor correctly aligned. Some cassettes contain a **grid** that reduces scattered radiation, improving image clarity. In digital radiography, the cassette converts X-ray energy into electrical signals, enabling high-resolution digital images.

2.9 Control Panel

The control panel is the operator's interface to the X-ray system. It displays technical parameters, exposure settings, and patient information. Operators adjust beam intensity, duration, and imaging protocols through buttons or touch controls. Built-in safety features—such as warning lights and emergency shutoff options—protect both patient and operator. The control panel ensures optimal image acquisition with minimal radiation dose.

2.10 X-Ray Film

X-ray film contains silver-halide-based emulsion layers that chemically react to X-ray exposure, forming a latent image which becomes visible after chemical development. Sensitizing agents increase its responsiveness, allowing detailed visualization of internal structures.

Because of its high sensitivity to radiation, X-ray film produces sharp images used for diagnostic evaluation.

2.11 CR Developer

In **Computed Radiography (CR)**, X-ray-exposed plates store a latent image that is later scanned by a laser beam within the CR reader. This scanning releases stored energy and converts it into digital signals. The CR developer processes these signals into a digital image using specialized software. Unlike DR systems, CR requires this additional scanning step to digitize the image.

2.12 DR Developer

Digital Radiography (DR) systems capture images instantly using flat-panel detectors. These detectors convert X-ray photons directly into electrical signals, eliminating the need for scanning. DR provides real-time imaging, faster workflow, and higher efficiency compared to CR.

2.13 Film Sizes

X-ray films are available in different dimensions according to clinical need:

- **8 × 10 in:** Hands, feet
- **11 × 14 in:** Limbs
- **14 × 17 in:** Chest, abdomen
- **17 × 19 in:** Spine, long bones

Selecting the appropriate size ensures full coverage of the anatomical region.

2.14 X-Ray Tube

The X-ray tube contains a **vacuum-sealed envelope**, a **tungsten cathode** emitting electrons, and a **metal anode** generating X-rays when struck by electrons. The focal spot directs the X-ray beam outward. The tube is designed to withstand high temperatures and voltage, ensuring consistent X-ray output.

3.Results and Discussion

Cortical break is seen affecting iliac blade and extending into acetabular roof is seen. No significant displacement of bone segments is seen. Joint is stable however fracture is extending into articular cavity through roof of the acetabulum

Impression

A 38-year-old patient presented with an acetabular fracture of the transverse type. The X- ray was taken at a 45-degree angle (Judet view) to assess the fracture more accurately. The transverse fracture type, which extends across the acetabulum, was identified, and the patient was evaluated and managed accordingly.

Figure 3.1: Right acetabular fracture x-ray image

Changes in intensity across a range of 0 to 400 are indicated by the fractured graph, which displays a greater and sharper peak in gray value (about 220) with more variations. The non-fractured graph, on the other hand, displays a more steady drop across a shorter distance of 0 to 300 and a smoother trend with lower gray values (around 140).

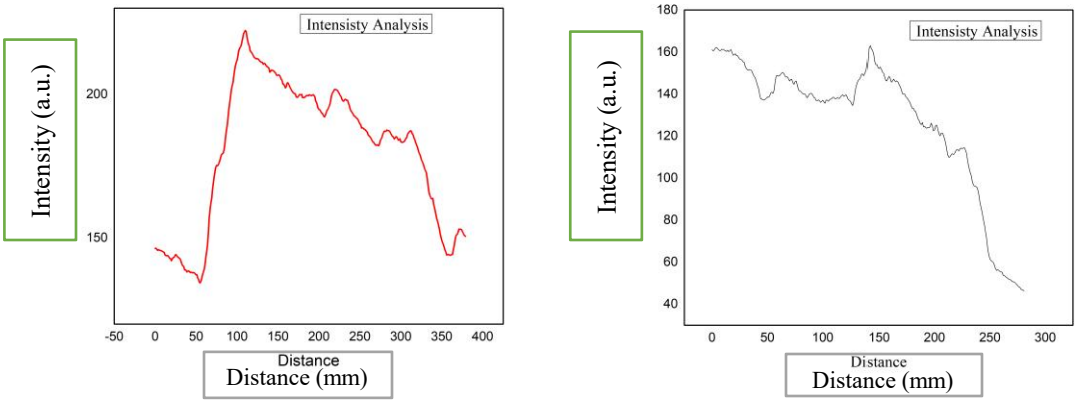

(a) Fractured (b)Non-Fractured

Figure 3.2: (a) and (b) intensity Analysis graph

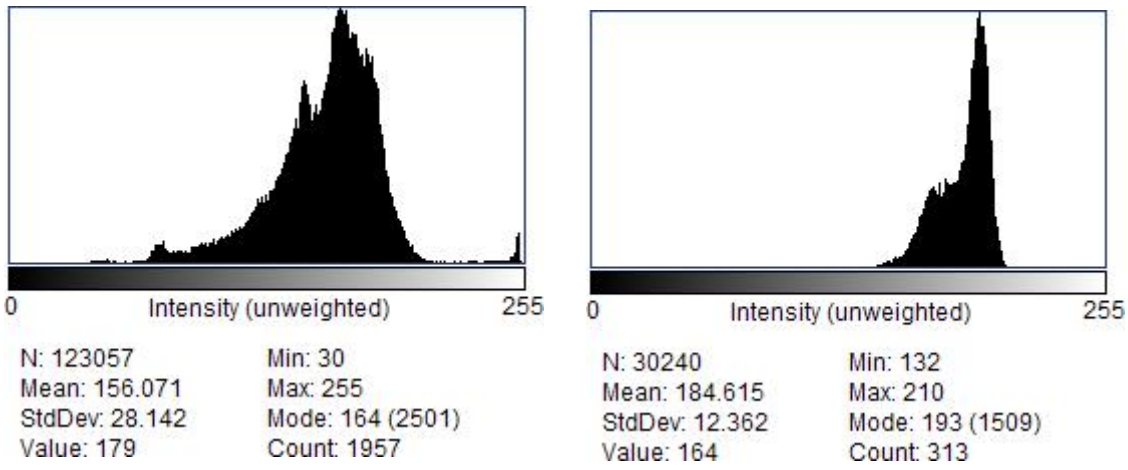

Fracture (a) Non-Fracture (b)

Figure 3.3: (a) and (b) Histogram of Acetabulum graph

Multiple fixators are seen along the lower lumbar spine, SI joint and pelvic ring in pelvis maintaining the reshaped pelvic ring, SI joint and lower lumbar vertebra. Healed fracture are seen along pubic rami, Sl joint and acetabular roof. Fixator is also seen in right femoral shaft with complete healing of the underlying fracture

Impression

Healed fractures with fixators in situ to maintain the re shaped anatomical integrity of pelvis.A 47-year-old patient presented with an acetabular fracture involving the reshaped. The X-ray was taken in the anteroposterior (AP) view at a 180-degree angle to properly assess the fracture. The re shaped fracture type was confirmed, and the patient was evaluated and treated accordingly.

Figure 3.4: Left acetabular roof and pubic symphysis bone fracture

Significant differences may be seen in the fractured graph, which displays abrupt peaks around a gray value of 130 across a distance of 500 pixels and larger intensity oscillations. There is less structural disruption in the Non-Fractured graph, which shows a smoother curve with smaller peaks that extends up to a gray value of 90 over a shorter distance of 200 pixels.

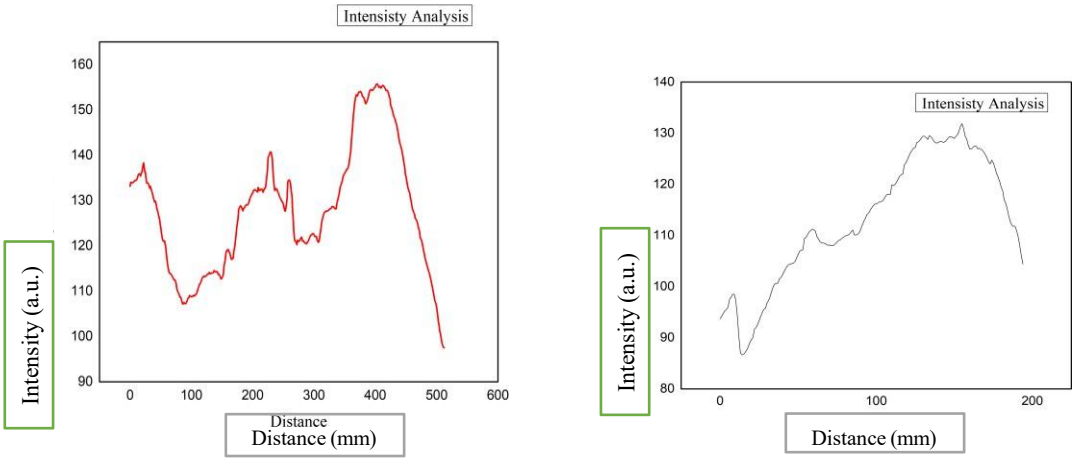

Fracture (a) Non-Fracture (b)

Figure 3.5: (a) and (b) intensity Analysis graph

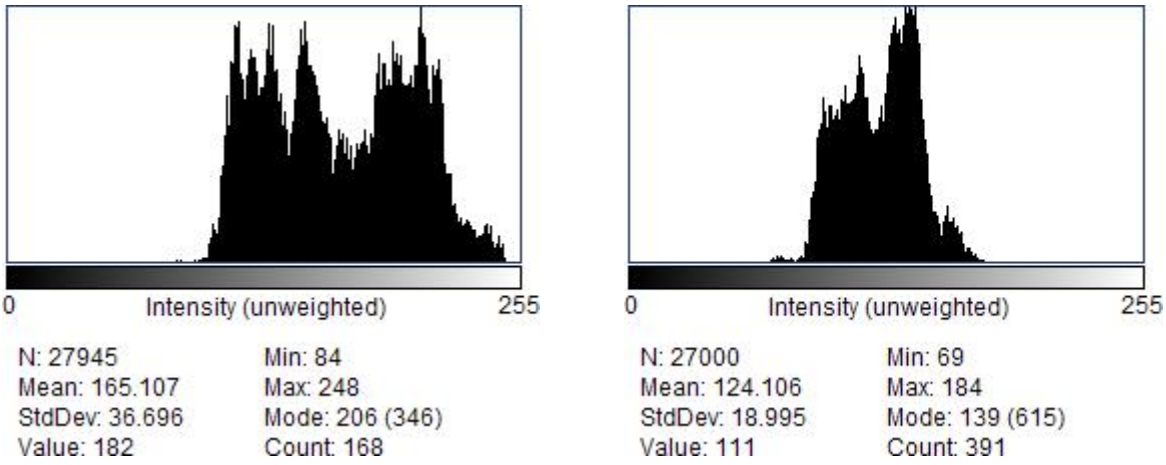

Fracture (a) Non-Fracture (b)

Figure 3.6: (a) and (b) Histogram of Acetabulum graph

Multiple fixator plates are seen in situ fixing posterior pillar as well as roof of acetabula. No air lucencies or inflammatory changes are seen. No particle disease is seen.Joint space is restored with some osteophytic activity suggestive of early osteoarthritic changes

Impression

A 28-year-old patient presented with an acetabular fracture involving the roof of acetabula. The X-ray was taken in the lateral view at a 90-degree angle to properly assess the fracture. The transverse fracture type was confirmed, and the patient was evaluated and treated accordingly.

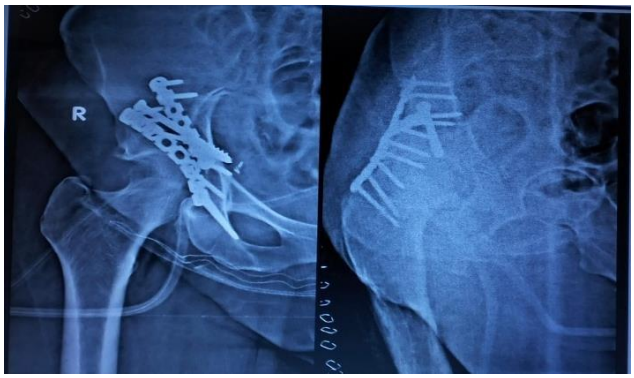

Figure 3.7: Right anterior and posterior fracture

The gray value intensity of fractured and non-fractured regions is contrasted in the graph. Higher variance and several peaks on the "Fractured" graph indicate anomalies brought on by the fracture. With fewer variations and a smoother curve with lower overall gray values, the "non-fractured" graph depicts a more homogeneous tissue structure free of fractures. This demonstrates how the two conditions differ visually.

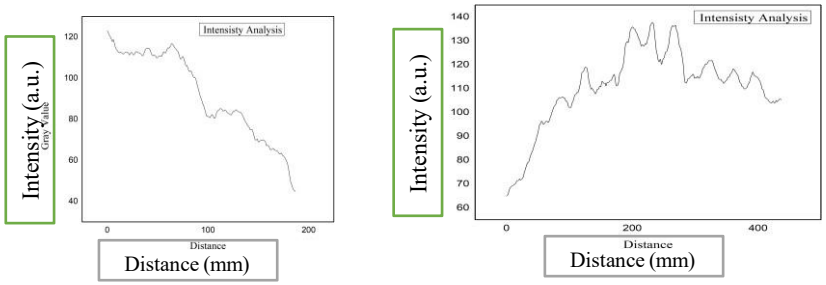

Fracture (a) fracture (b)

Figure 3.8: (a) and (b) intensity Analysis graph

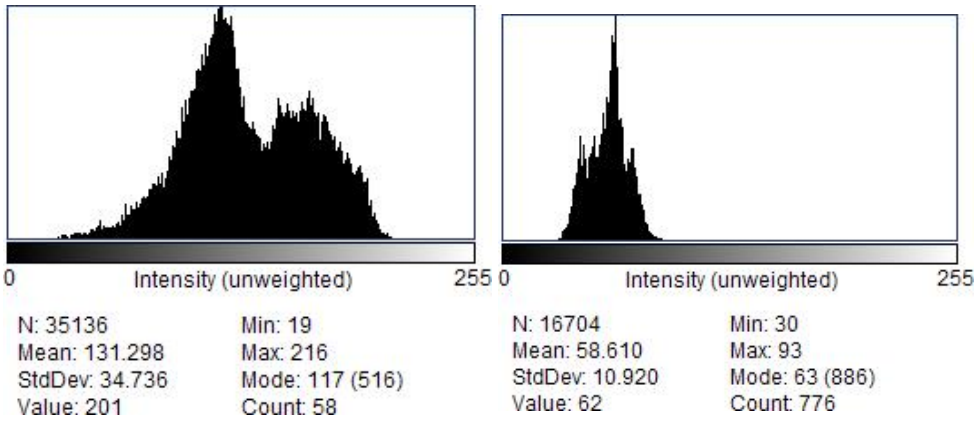

Fracture (a) Non-Fracture (b)

Figure 3.9: (a) and (b) Histogram of Acetabulum graph

Comminuted fracture of proximal end of left femur is seen. Fracture line is passing through inter trochanteric region. There is element of upward displacement of distal femoral segment. Few fragments are lying along the neck of femur and acetabulum posterior wall

Impression

Findings are suggestive of comminuted intertrochanteric fracture of neck of femur and injury of posterior wall. The patient was 75 years old and had an acetabular fracture affecting the posterior wall and a transverse fracture of the neck of the femur. The patient was positioned at a 180-degree angle for the anteroposterior (AP) view of the neck of the femur, with a 45- degree angle for the acetabulum. The fracture was confirmed at 100%.

Figure 3.10: Proximal end of left femur

The fractured and non-fractured material graphs show variations in intensity over a predetermined distance. Damage or anomalies are shown by greater intensity variation in the broken graph (left). A more consistent and undamaged structure is indicated by the non- fractured graph's (right) smoother, more consistent intensity shifts. These patterns of fluctuation in intensity represent the structural integrity of each substance.

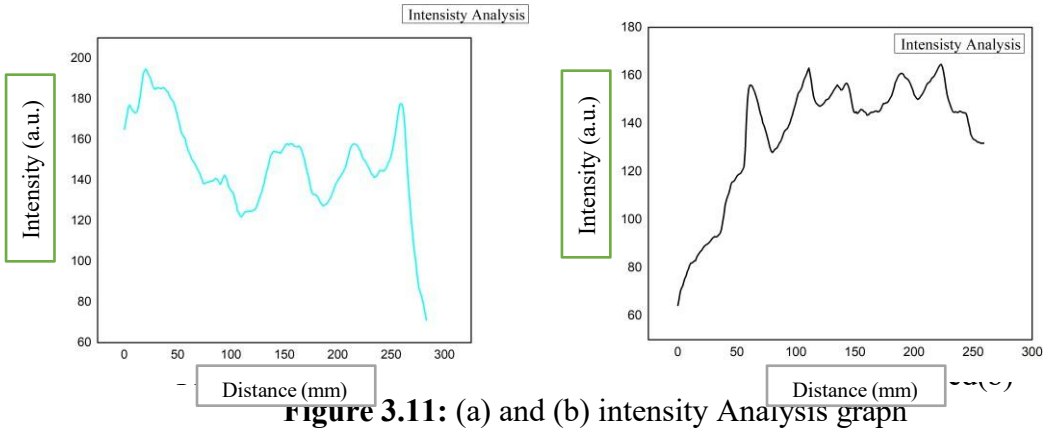

Figure 3.11: (a) and (b) intensity Analysis graph

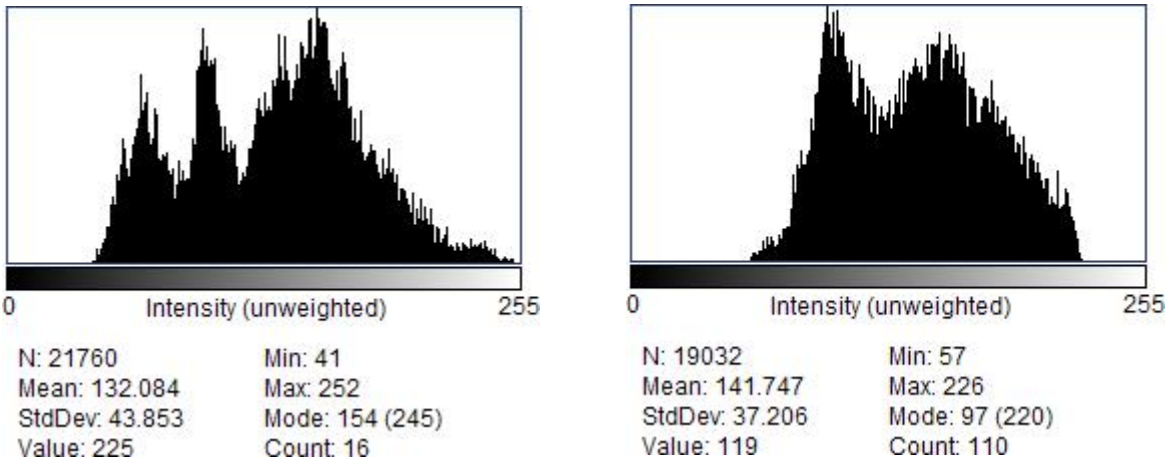

Fracture (a) Non-Fracture (b)

Figure 3.12: (a) and (b) Histogram of Acetabulum graph

Multiple fixator plates are seen in situ fixing anterior pillar as well as roof of acetabula. No air lucencies or inflammatory changes are seen. No particle disease is seen. Central nail is seen passing through the femoral head into acetabulum either for fixation of joint or artefactual placement. Joint space is reduced with element of some fusion and adjacent osteophytic activity suggestive of Joint arthrosis and early osteoarthritic changes. The patient was 55 years old and had an acetabular fracture involving the anterior wall, classified as a T-shaped type. The patient was positioned at a 45-degree for the lateral view . The fracture was confirmed at 100%.

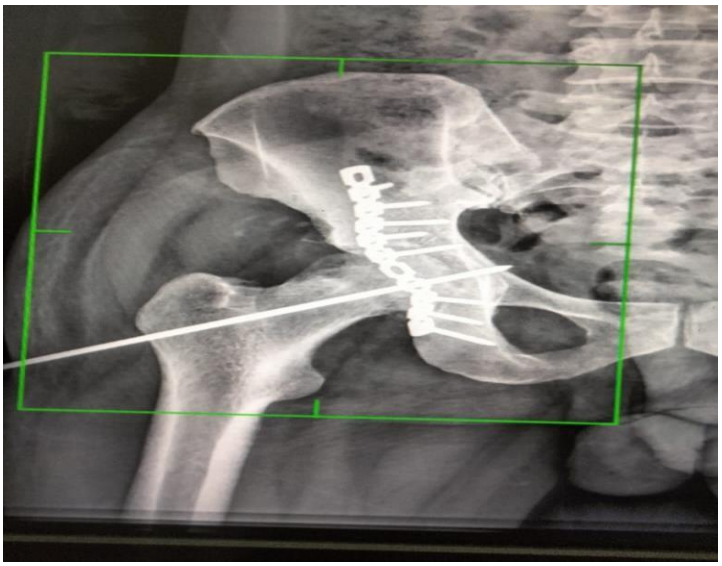

Figure 3.13: Anterior pillar as well as roof of acetabulum fracture

Grey value intensity for fractured and non-fractured surfaces is contrasted in the graphs. Different surface irregularities typical of shattered material are indicated by the fracture graph's uneven peaks and dips. The smoother, more progressive increase of the non-fracture

graph, on the other hand, indicates a more uniform surface devoid of abrupt changes, which is characteristic of an undamaged material

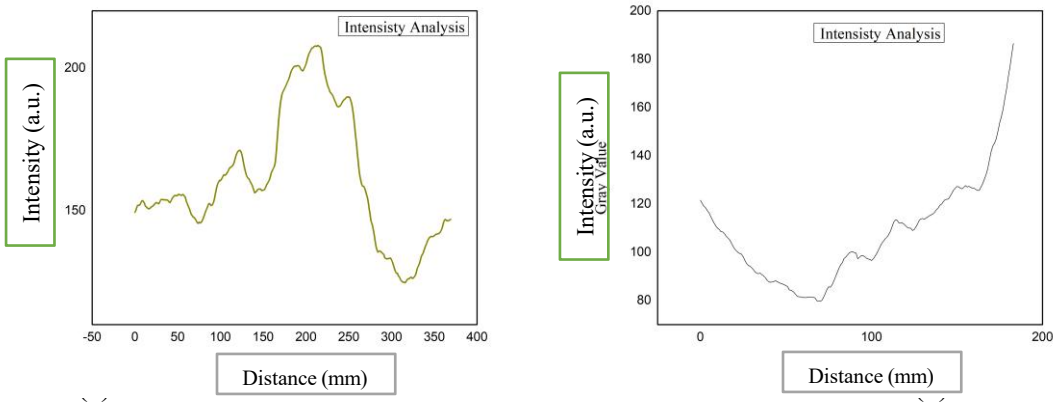

Fr

Figure 3.14: (a) and (b) intensity Analysis graph

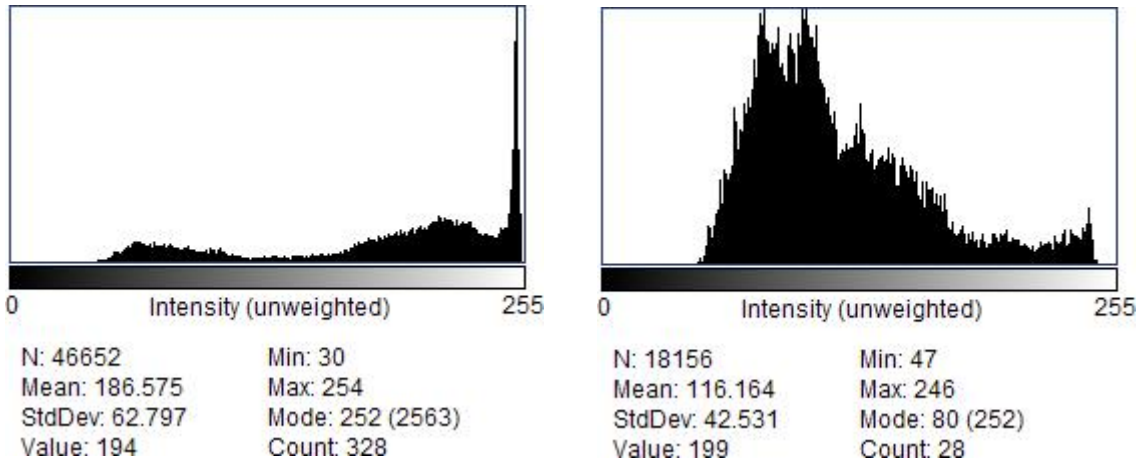

Fracture (a) Non-Fracture (b)

Figure 3.15: (a) and (b) Histogram of Acetabulum graph

Sutural diastasis of symphysis pubis is seen with wide separation of body of pubis bone. Fracture of superior and inferior pubic rami is seen on right side. Right Hip joint disruption is seen with superior dislocation of righ femoral head. Acetabular roof fracture is also seen

Impression

Findings are suggestive of Open Book Fracture with Hip dislocation and public as well acetabular roof fractures. The patient was 28 years old and had superior and inferior pubic fractures. The patient was positioned at a 47-degree angle, and the acetabulum roof was also observed. The fractures were confirmed at 100%.

Figure 3.16: Acetabular roof fracture and inferior pubic rami

Over distance, the fractured and non-fractured graphs display patterns of intensity. Intensity increases, decreases, and fluctuates repeatedly in the broken sample (left), suggesting surface damage or irregularity. A more homogeneous and stable structure is suggested by the non-fractured sample's (right) smoother, steadier rise and fewer oscillations.

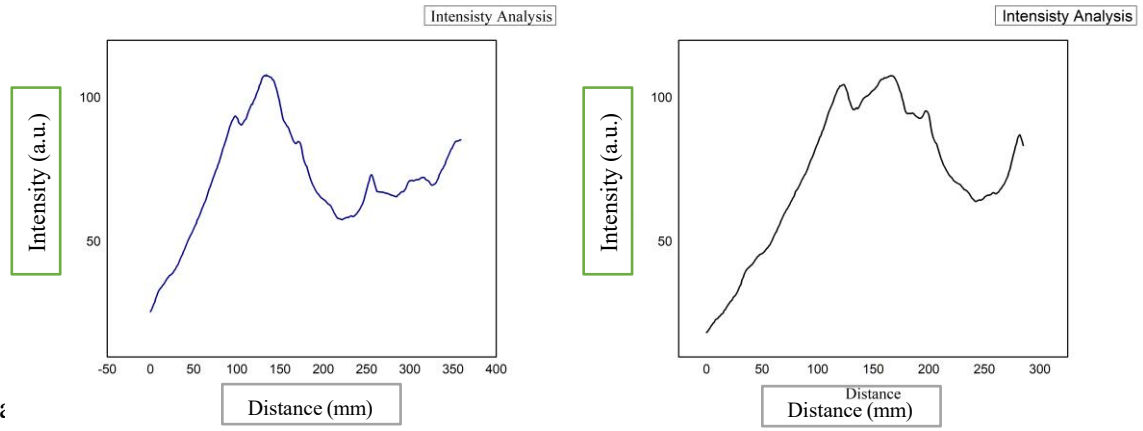

Fra

Figure 3.17: (a) and (b) intensity Analysis graph

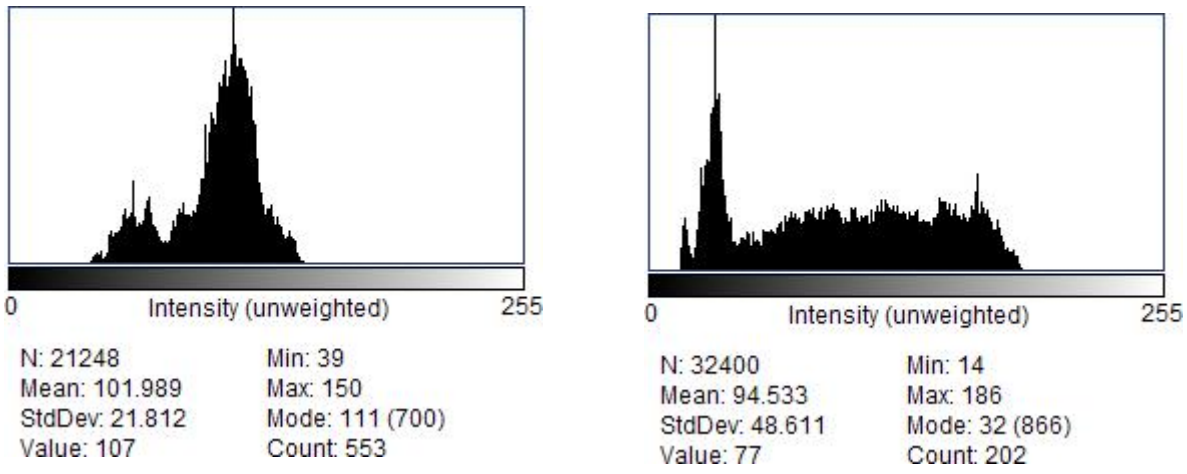

Fracture (a) Non-Fracture (b)

Figure 3.18: (a) and (b) Histogram of Acetabulum graph

Fracture and dislocation of right femoral neck is seen with superior displacement of distal segment. Femoral head shows bone loss and erosions and is suggestive of avascular bone necrosis. Loss of Joint congruity with abundant osteophytes suggest chronic process

Impression

Findings are suggestive of chronic fracture neck of femur with its sequel of AVN and advanced osteoarthiritis and joint remodeling. The patient was 65 years old and had fractures involving the anterior wall of the acetabulum and the neck of the femur. The fractures were confirmed at 100%.

Figure 3.19: had fractures involving the anterior wall of the acetabulum and the neck of the femur

Intensity analyses are displayed in the two graphs, which compare gray values across distance. With gray values ranging from 130 to more than 600, the first graph exhibits greater fluctuation, indicating greater intensity variance. With gray values ranging from 170 to 200,

the second graph shows less fluctuation and is smoother. Both figures show variations in brightness over a given distance, but they vary in intensity to varying degrees.

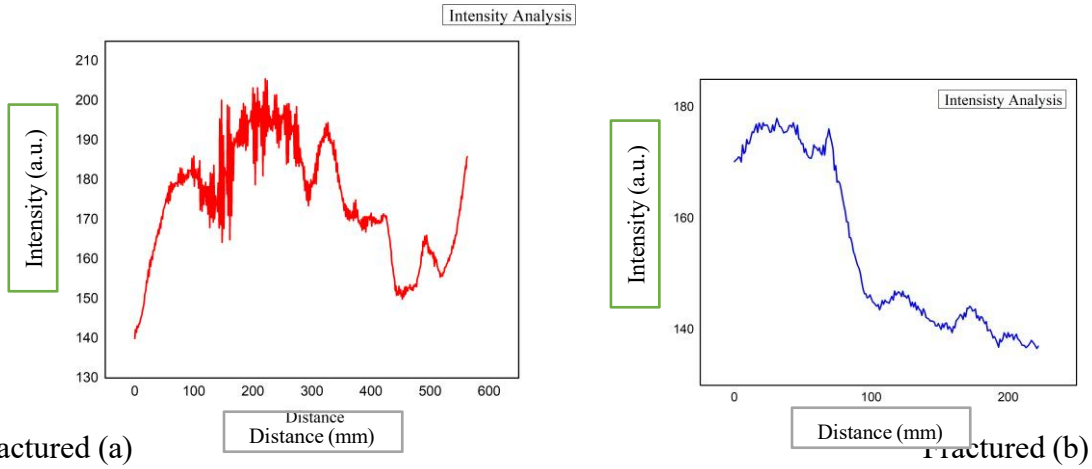

Fractured (a) Fractured (b)

Figure 3.20: (a) and (b) intensity Analysis graph

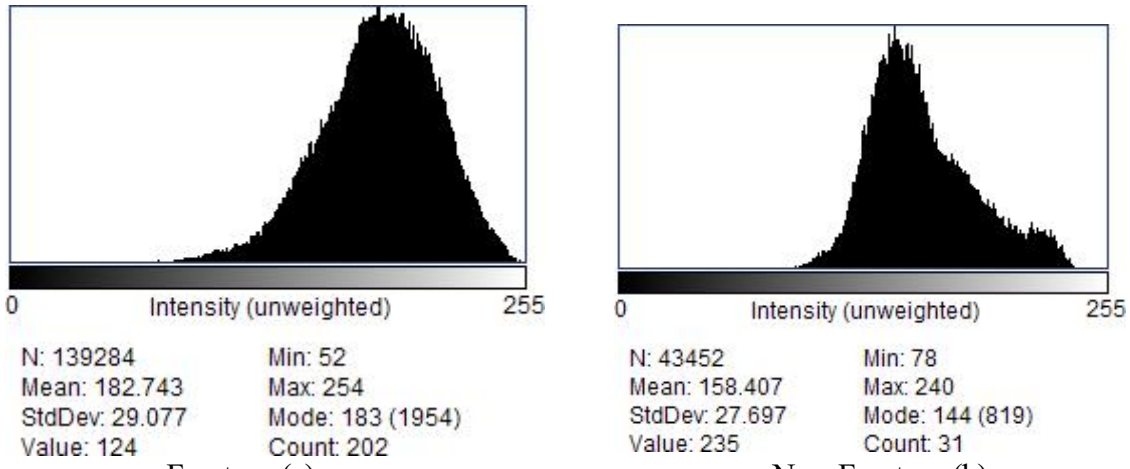

Fracture (a) Non-Fracture (b)

Figure 3.21: (a) and (b) Histogram of Acetabulum graph

Healing fracture of inferior right pubic arch as well as superior arch is seen along with fracture and medial displacement of contralateral iliac bone fracture line is passing through acetabular roof Findings are suggestive of left lateral compression fracture

Figure 3.22: inferior right pubic and acetabular roof fracture

Two graphs comparing the intensity of gray values for fractured and non-fractured samples with distance are displayed in the image: Fractured: As distance increases, the blue line shows varying gray values that progressively get smaller. The black line is non-fractured; it increases steadily, peaks about 220, and then levels off with hardly little fluctuations. In conclusion, the non-fractured sample exhibits a smoother increase and stabilization, whereas the fractured sample exhibits more erratic variations.

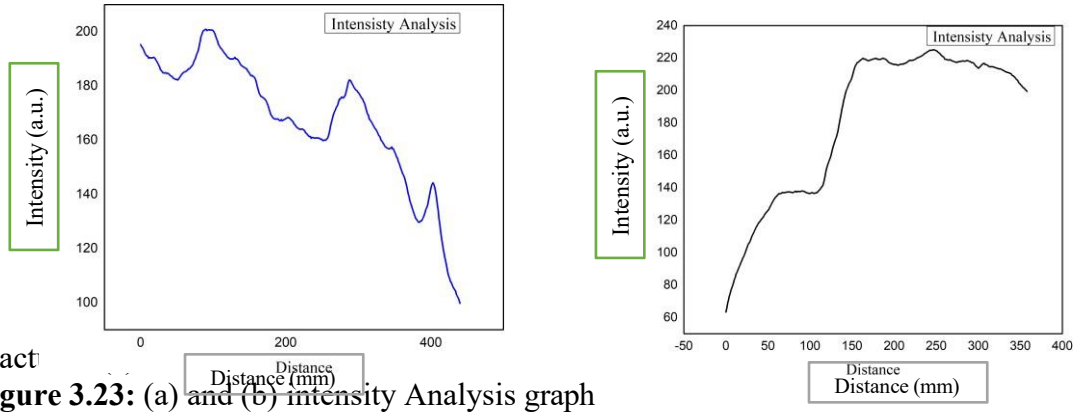

Fract

Figure 3.23: (a) and (b) intensity Analysis graph

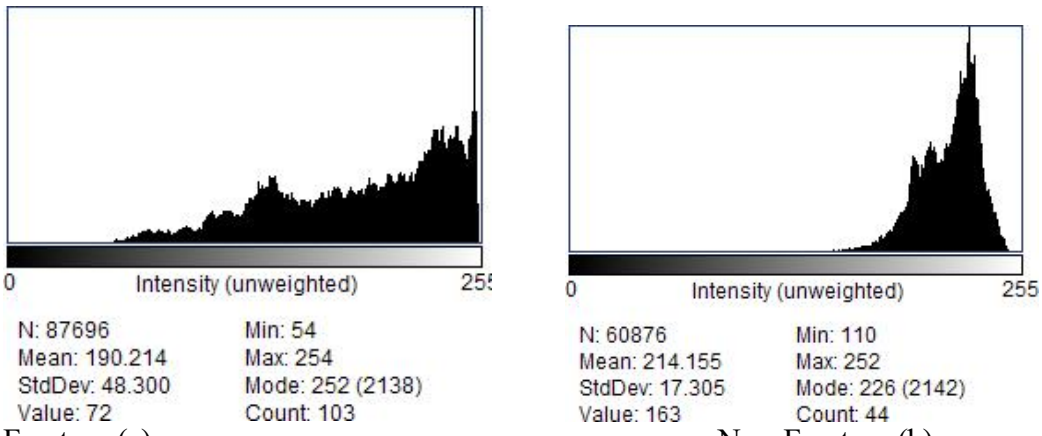

Fracture (a) Non-Fracture (b)

Figure 3.24: (a) and (b) Histogram of Acetabulum graph

Multiple fractures are seen affecting innominate bones just above the hip joint affecting iliac blade, acetabulum associated with Diastasis of right Sl joint and associated sacral bone fracture -----

CONCLUSION:

Findings are suggestive of Lateral compression fracture. The patient was 38 years old and had multiple fractures, classified as transverse and oblique types. The patient was positioned at angles of 45, degrees for the anteroposterior (AP) and lateral view (LA). The assessment confirmed the fractures at 100%.

Figure 3.25: Multiple acetabular fracture

Two graphs showing the intensity analysis of gray values over distance for samples that are broken and those that are not are displayed in the image: Fractured: The gray value of the red line rises sharply, reaching a high of about 200, and then falls. Non-Fractured: The gray

line exhibits a slow decline in gray values together with more modest variations. In general, the non-fractured sample shows smoother fluctuations, but the fractured sample displays a more abrupt peak and decrease.

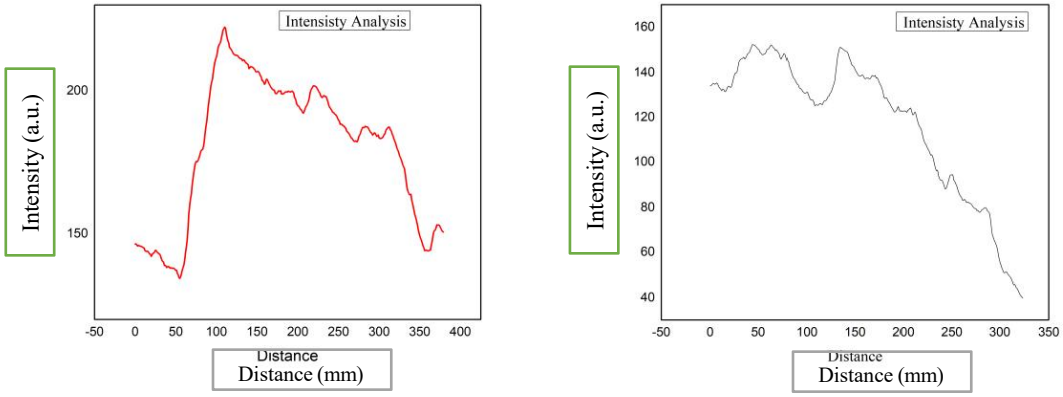

Fr

Figure 3.26: (a) and (b) intensity Analysis graph

Fractured Non-Fractured

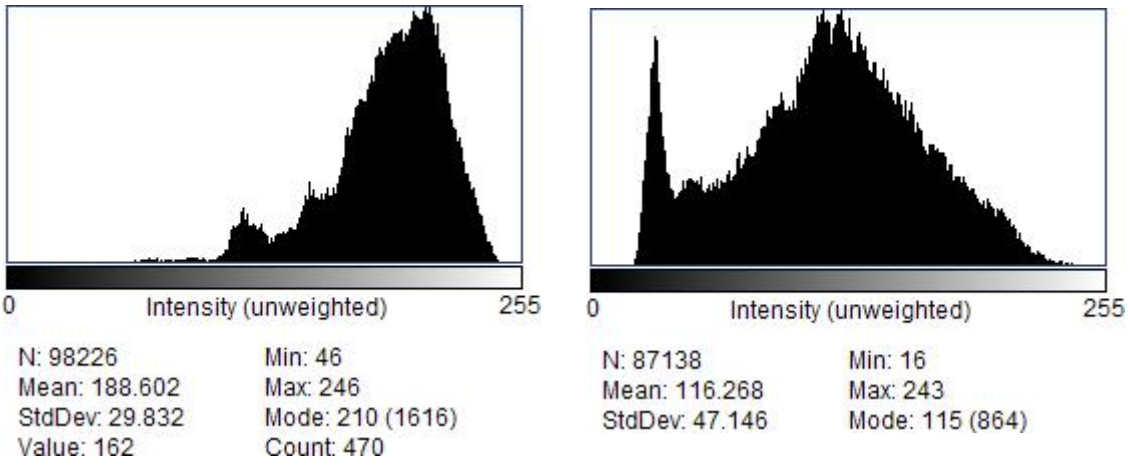

Fracture (a) Non-Fracture (b)

Figure 3.27: (a) and (b) Histogram of Acetabulum graph

Total hip replacement is carried out and hip prosthesis is seen in situ. No particle disease or infection is seen.Healing fracture is seen in pelvic inlet rim outline.

CONCLUSION:

Associated early osteoarthiritic changes are seen.The patient was 66 years old and had undergone a complete hip replacement, with no acetabular fracture observed. The patient was positioned at a 90-degree for the lateral view (LA), and the assessment confirmed no fractures at 100%.

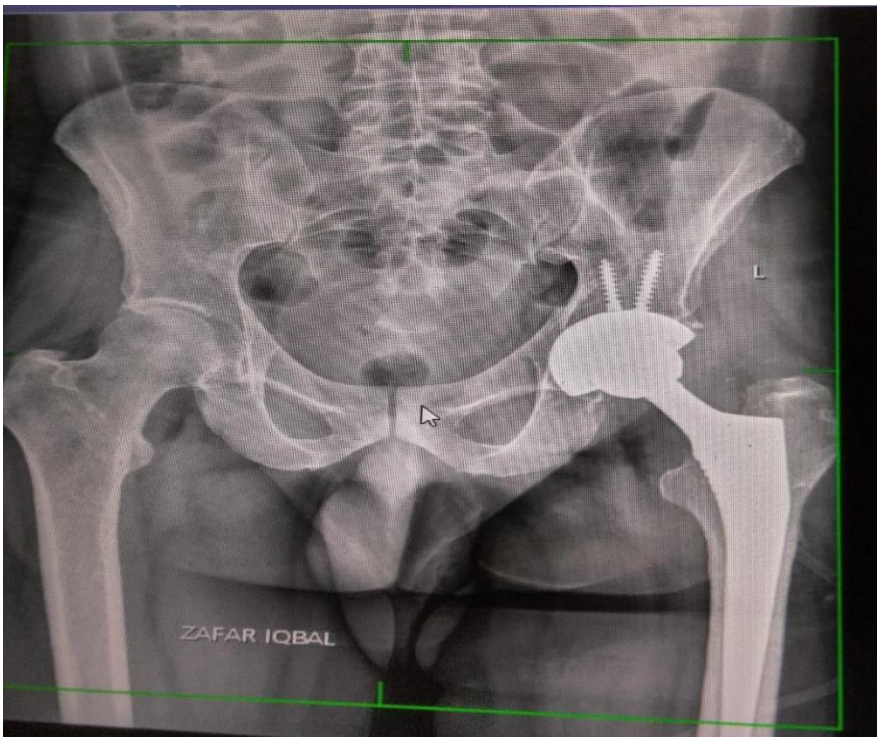

Figure 3.28: Total hip replacement

The above graphic displays two graphs that compare the intensity of the gray value for fractured and non-fractured materials over a specific distance. Fractured: A more gradual shift is suggested by the red line graph's reduced gray value variance. Non-fractured: The intensity varies more in the blue line graph, suggesting higher surface variability. According to this comparison, there are more abnormalities in the non-fractured material whereas the fractured material exhibits smoother intensity changes.

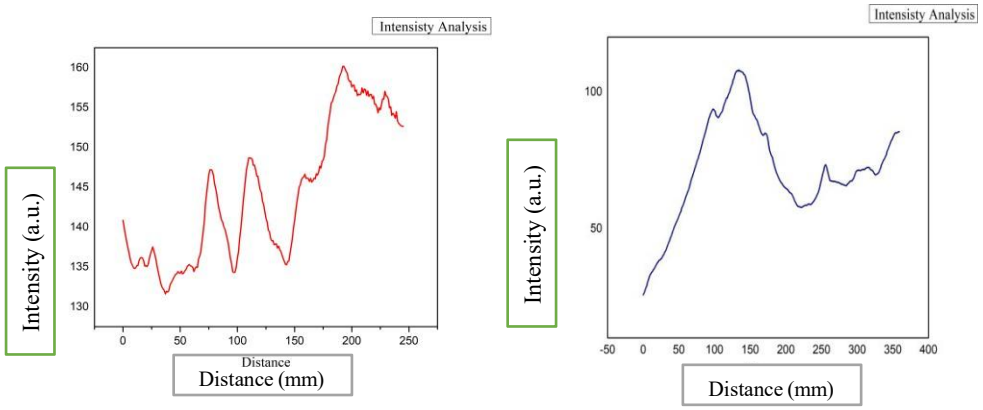

Fractured (a) Non-fractured (b)

Figure 3.29: (a) and (b) intensity Analysis graph

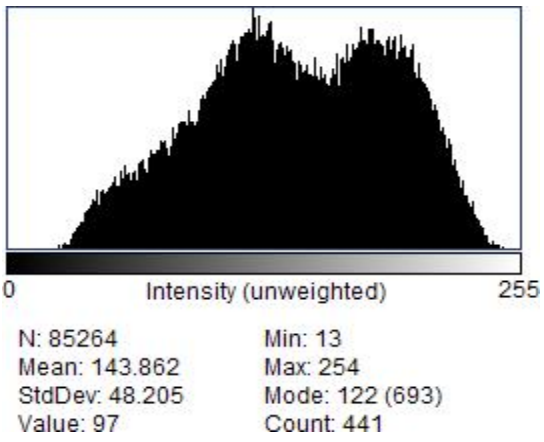

Fracture (a)

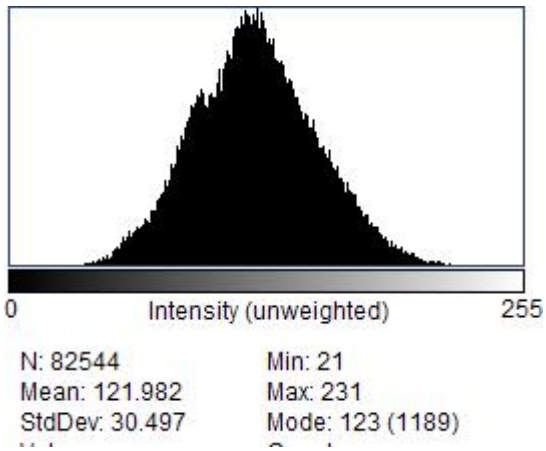

Non-Fracture (b)

Figure 3.30: (a) and (b) Histogram of Acetabulum graph

Open book fractures are seen affecting bilateral superior, inferior pubic archs, acetabular roof and diastasis of left SI joints

These fractures are causing distortion and dis-alignement of weight bearing joints.The patient was 57 years old and had an acetabular fracture involving bilateral superior and inferior pubic regions, classified as Anterior column and posterior hemi-transvers type. The patient was positioned at a 46-degree lateral angle for the lateral view (LA), and the fracture was confirmed at 100%(Tassani & Matsopoulos, 2014).

Figure 3.31: Bilateral superior, inferior pubic archs, acetabular roof

The first graph, called "Fracture," has significant intensity fluctuation, which is typical of fra ion-

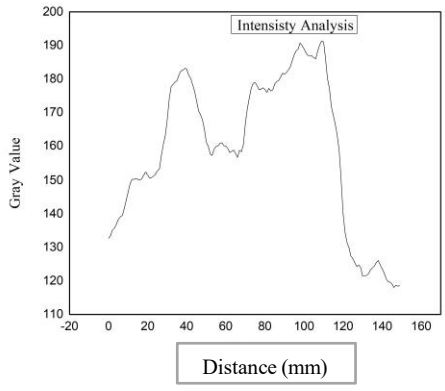

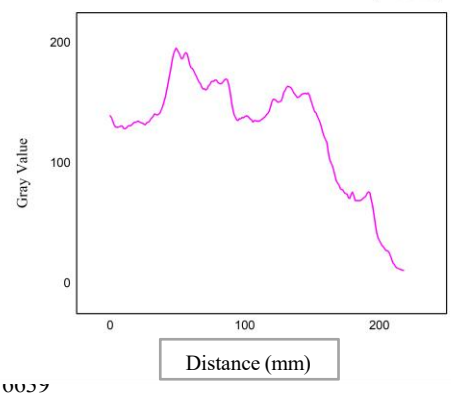

fracture," suggests less variance and less consistent intensity, which are traits of non-fractured areas.

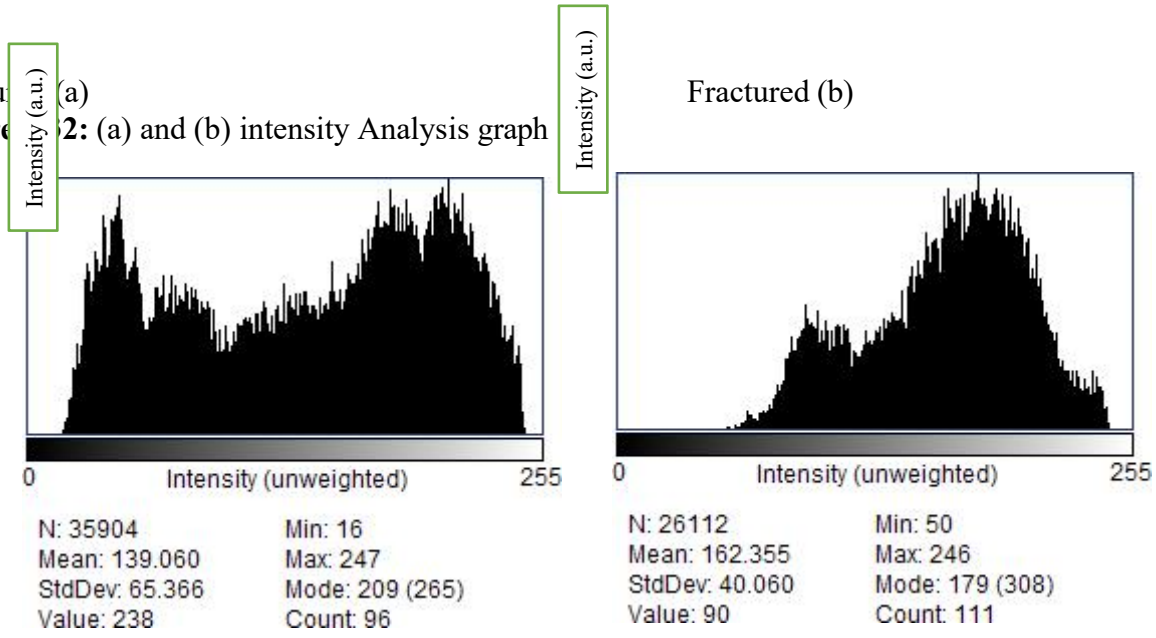

Fractu (a) Fractured (b)

Figure 2: (a) and (b) intensity Analysis graph

Fracture (a) Non-Fracture (b)

Figure 3.33: (a) and (b) Histogram of Acetabulum graph

4.Conclusions

- The assessment of acetabular fractures significantly improves when the rotational angle in Judet view X-ray imaging is optimized.
- Measurement errors are reduced, and inter-observer agreement is enhanced.
- Fracture morphology is most accurately visualized at a 45° rotational angle.
- Standardizing the Judet view procedure at this angle can improve patient outcomes by enabling precise diagnoses and well-informed treatment decisions.
- These findings highlight the importance of standardized imaging protocols in orthopedic trauma management.

5. References

Castaneda, C., Nalley, K., Mannion, C., Bhattacharyya, P., Blake, P., Pecora, A., . . . Suh, K. S. (2015). Clinical decision support systems for improving diagnostic accuracy and achieving precision medicine. *Journal of clinical bioinformatics, 5*(1), 4.

Dreizin, D., LeBedis, C. A., & Nascone, J. W. (2019). Imaging acetabular fractures. *Radiologic Clinics, 57*(4), 823-841.

Garbe, C., & Sharma, R. (2024). Multiomics technologies to increase resilience, adaptability, and affordability of integrated traditional and modern healthcare. In *Resilient health* (pp. 155-164): Elsevier.

Glaser, C., D'Anastasi, M., Theisen, D., Notohamiprodjo, M., Horger, W., Paul, D., & Horng, A. (2015). *Understanding 3D TSE sequences: advantages, disadvantages, and application in MSK imaging.* Paper presented at the Seminars in Musculoskeletal Radiology.

Kelly, J., Ladurner, A., & Rickman, M. (2020). Surgical management of acetabular fractures–a contemporary literature review. *Injury, 51*(10), 2267-2277.

Martinec, D., & Pajdla, T. (2007). *Robust rotation and translation estimation in multiview*

reconstruction. Paper presented at the 2007 IEEE conference on computer vision and pattern recognition.
Mercer, D. K., & Stewart, C. S. (2019). Keratin hydrolysis by dermatophytes. *Medical mycology, 57*(1), 13-22.
Morgenstern, M., Kühl, R., Eckardt, H., Acklin, Y., Stanic, B., Garcia, M., . . . Metsemakers, W.-J. (2018). Diagnostic challenges and future perspectives in fracture-related infection. *Injury, 49*, S83-S90.
Popa, M., Cursaru, A., Cretu, B., Iordache, S., Iacobescu, G. L., Spiridonica, R., . . . Iacobescu Sr, G. L. (2024). Enhancing osteoporosis management: a thorough examination of surgical techniques and their effects on patient outcomes. *Cureus, 16*(5).
Tassani, S., & Matsopoulos, G. K. (2014). The micro-structure of bone trabecular fracture: an inter-site study. *Bone, 60*, 78-86.
Tazeabadi, S. A., Noroozi, S. G., Salehzadeh, M., Bahardoust, M., Farahini, H., Hajializade, M., & Yeganeh, A. (2020). Evaluation of Judet view radiographs accuracy in classification of acetabular fractures compared with three-dimensional computerized tomographic scan: a retrospective study. *BMC Musculoskeletal Disorders, 21*(1), 405.
Teja, T., Shrivastava, S., Choudhary, A., Rathod, V., & Balusani, P. (2024). Optimizing acetabular positioning: a comprehensive review of contemporary strategies in total hip arthroplasty. *Cureus, 16*(4).
Tigani, D., Lamattina, L., Assenza, A., Melucci, G., Pizzo, A., & Donadono, C. (2025). Management of Acetabular Fractures with Total Hip Replacement: A Narrative Literature Review. *Journal of Personalized Medicine, 15*(7), 282.